PREPARED FOR THE U.S. DEPARTMENT OF ENERGY,
UNDER CONTRACT DE-AC02-76CH03073

**PPPL-3890**
UC-70

**PPPL-3890**

# MHD Ballooning Instability in the Plasma Sheet

by
C.Z. Cheng and S. Zaharia

October 2003

PPPL
PRINCETON PLASMA
PHYSICS LABORATORY

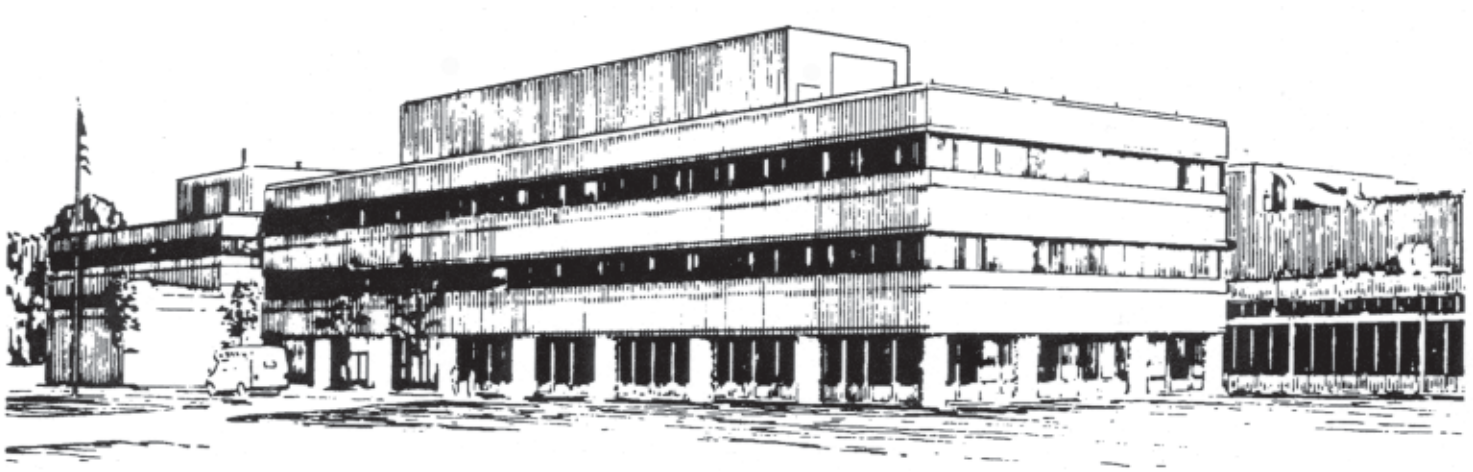

**PRINCETON PLASMA PHYSICS LABORATORY**
**PRINCETON UNIVERSITY, PRINCETON, NEW JERSEY**

## PPPL Reports Disclaimer



## Availability

This report is posted on the U.S. Department of Energy's Princeton Plasma Physics Laboratory Publications and Reports web site in Fiscal Year 2004. The home page for PPPL Reports and Publications is: http://www.pppl.gov/pub_report/

DOE and DOE Contractors can obtain copies of this report from:

U.S. Department of Energy
Office of Scientific and Technical Information
DOE Technical Information Services (DTIS)
P.O. Box 62
Oak Ridge, TN 37831

Telephone: (865) 576-8401

Fax: (865) 576-5728

Email: reports@adonis.osti.gov

This report is available to the general public from:

National Technical Information Service
U.S. Department of Commerce
5285 Port Royal Road
Springfield, VA 22161

Telephone: 1-800-553-6847 or
(703) 605-6000

Fax: (703) 321-8547

Internet: http://www.ntis.gov/ordering.htm

# MHD Ballooning Instability in the Plasma Sheet

C. Z. Cheng
Princeton Plasma Physics Laboratory, Princeton University, Princeton, NJ 08543

S. Zaharia
Los Alamos National Laboratory, Los Alamos, NM 87545

Received _____; accepted _____

Short title: BALLOONING INSTABILITY

**Abstract.** Based on the ideal MHD model the stability of ballooning modes is investigated by employing realistic 3D magnetospheric equilibria, in particular for the substorm growth phase. Previous MHD ballooning stability calculations making use of approximations on the plasma compressibility can give rise to erroneous conclusions. Our results show that without making approximations on the plasma compressibility the MHD ballooning modes are unstable for the entire plasma sheet where $\beta_{eq} \geq 1$, and the most unstable modes are located in the strong cross-tail current sheet region in the near-Earth plasma sheet, which maps to the initial brightening location of the breakup arc in the ionosphere. However, the MHD $\beta_{eq}$ threshold is too low in comparison with observations by AMPTE/CCE at $X = -(8-9)\,\mathrm{R_E}$, which show that a low frequency instability is excited only when $\beta_{eq}$ increases over 50. The difficulty is mitigated by considering the kinetic effects of ion gyroradii and trapped electron dynamics, which can greatly increase the stabilizing effects of field line tension and thus enhance the $\beta_{eq}$ threshold [*Cheng and Lui*, 1998]. The consequence is to reduce the equatorial region of the unstable ballooning modes to the strong cross-tail current sheet region where the free energy associated with the plasma pressure gradient and magnetic field curvature is maximum.

## 1. Introduction

Observations by AMPTE/CCE satellite have clearly demonstrated that toward the end of late growth phase in the near-Earth plasma sheet region the plasma pressure becomes isotropic and $\beta = 2P/B^2$ increases to $\geq 50$ and a low frequency instability with a wave period of $\sim 50 - 75$ seconds (in the Pi 2 frequency range) is excited and grows exponentially to a large amplitude and causes the onset of current disruption [*Cheng and Lui*, 1998]. It is emphasized that the initial excitation of the low frequency instability occurs in a localized equatorial area of less than 1 $R_E$ in width in the near-Earth plasma sheet region [*Ohtani et al.*, 1991]. The low frequency modes have also been observed by satellites not located at the initiation region during the substorm expansion phase [e.g., *Roux et al.*, 1991; *Erickson et al.*, 2000].

To explain the observed low frequency instability, theoretical investigations of the ballooning instability based on the ideal MHD model have been made [e.g., *Lee and Wolf*, 1992; *Hurricane*, 1997; *Lee*, 1998; *Horton et al.*, 1999; *Lee*, 1999]. All these previous ideal calculations employed simplified equilibria in 2D magnetospheric geometries and made simplified assumptions on the plasma compressibility to reduce the eigenmode equations from a fourth order differential equation to a second order integro-differential equation. The stability of ballooning modes depends crucially on the equilibrium field structure and the assumption made on the plasma compressibility. Numerical calculations to examine the compressibility effect with different simplifying assumptions of the plasma compressibility [*Lee*, 1999] have been performed for a 2D equilibrium model by *Voigt* [1986]. By assuming the parallel plasma displacement to be a constant along the field line [*Lee and Wolf*, 1992], the stability calculations predicted a low $\beta$ ($\leq 1$) threshold for instability. *Horton et al.* [1999] considered a different approximation for the plasma compressibility with the fast-MHD model which assumes that the wave propagates very fast along the ambient magnetic field such that there is not sufficient time for parallel plasma motion and the plasma displacement along $\mathbf{B}$ vanishes, and they concluded that

the ballooning instability occurs for $\beta < 1$. However, the numerical stability calculations of the fast-MHD model performed by *Lee* [1999] show that the ballooning mode is stable in the Voigt's equilibrium, which is in contradiction to the analytical conclusion of *Horton et al.* [1999]. Calculations with these simplifying compressibility models, but with a more stretched 2D equilibrium field model by *Kan* [1973] gave totally different results from the Voigt's equilibrium. These results clearly illustrate that to obtain the correct stability result even within the ideal MHD model it is essential to model the plasma compressibility correctly as well as the equilibrium fields realistically. Another drawback of these previous ballooning stability calculations is that there is no information on where in the equatorial plane the ballooning instability would be unstable because of the use of 2D equilibria.

In this paper we will investigate the ballooning instability based on the ideal MHD model without making assumptions on plasma compressibility. Moreover, we will employ realistic 3D growth phase magnetospheric equilibria that satisfy the force balance, which should provide the valuable information of where in the plasma sheet the free energy and the most unstable ballooning instability are located. Our results show that the ballooning stability calculations making use of approximations on the plasma compressibility can give rise to erroneous conclusions. Based on the full MHD model our results show that the ballooning instability is most unstable in the strong cross-tail current sheet region in the near-Earth plasma sheet, which maps to the initial brightening location of the breakup arc in the ionosphere.

## 2. Ideal MHD Theory of Ballooning Instability

We first derive the ideal MHD eigenmode equations without making assumption on the plasma compressibility. We consider quasi-static equilibria with the equilibrium relations $\mathbf{J} \times \mathbf{B} = \boldsymbol{\nabla} P$ and $\boldsymbol{\nabla}(P + B^2/2) = \boldsymbol{\kappa} B^2$, where $\boldsymbol{\kappa} = (\mathbf{B}/B) \cdot \boldsymbol{\nabla}(\mathbf{B}/B)$ is the magnetic field curvature vector. With the time dependence of perturbed quantities as

$e^{-i\omega t}$, the linearized ideal MHD equations governing the asymptotic behaviors of the perturbed quantities are the momentum equation, $\rho\omega^2\boldsymbol{\xi} = \boldsymbol{\nabla}\delta P + \delta\mathbf{B}\times\mathbf{J} + \mathbf{B}\times\delta\mathbf{J}$, the adiabatic pressure law, $\delta P + \boldsymbol{\xi}\cdot\boldsymbol{\nabla}P + \Gamma_s P\boldsymbol{\nabla}\cdot\boldsymbol{\xi} = 0$, the Ampere's law, $\boldsymbol{\nabla}\times\delta\mathbf{B} = \delta\mathbf{J}$, the Faraday's law, $-i\omega\delta\mathbf{B} = \boldsymbol{\nabla}\times\delta\mathbf{E}$, and the Ohm's law, $\delta\mathbf{E} = i\omega\boldsymbol{\xi}\times\mathbf{B}$, where $\boldsymbol{\xi}$ is the usual fluid displacement vector, $\delta\mathbf{B}$ is the perturbed magnetic field, $\delta P$ is the perturbed plasma pressure, $\rho$ is the total plasma mass density, $\delta\mathbf{E}$ is the perturbed electric field, and $\Gamma_s = 5/3$ is the ratio of specific heats. We introduce the electrostatic potential $\phi$ and the vector potential $\mathbf{A}$ such that the perturbed electric field is expressed as $\delta\mathbf{E} = -\boldsymbol{\nabla}\phi + i\omega\mathbf{A}$, and the perturbed magnetic field as $\delta\mathbf{B} = \boldsymbol{\nabla}\times\mathbf{A}$. Because the perturbed parallel electric field vanishes in the ideal MHD model, we have $A_\parallel = \mathbf{A}\cdot\mathbf{B}/B = -\mathbf{B}\cdot\boldsymbol{\nabla}\Phi/B$, where $\Phi = i\phi/\omega$. We also assume that $A_\parallel$ and $\mathbf{A}_\perp$ are of the same order, but $|\boldsymbol{\nabla}_\perp\phi| \gg |\boldsymbol{\nabla}_\parallel\phi|$. Then, $\delta\mathbf{E}_\perp \simeq -\boldsymbol{\nabla}_\perp\phi$ and $\boldsymbol{\xi}\times\mathbf{B} \simeq \boldsymbol{\nabla}_\perp\Phi$.

Operating on the momentum equation with $\mathbf{B}\times$, we obtain the perturbed current density perpendicular to $\mathbf{B}$, and we have

$$\boldsymbol{\nabla}\cdot\delta\mathbf{J}_\perp \simeq \frac{\rho\omega^2}{B^2}\nabla_\perp^2\Phi - \frac{2\boldsymbol{\kappa}\times\mathbf{B}\cdot\boldsymbol{\nabla}\delta P}{B^2} - \frac{\mathbf{B}\times\boldsymbol{\nabla}P}{B^4}\cdot\boldsymbol{\nabla}(\delta P + \delta\mathbf{B}\cdot\mathbf{B}), \tag{1}$$

where the small term $\delta\mathbf{B}\cdot\boldsymbol{\nabla}(\mathbf{J}\cdot\mathbf{B}/B^2)$ is neglected. Next, we choose the Coulomb gauge $\boldsymbol{\nabla}\cdot\mathbf{A} = 0$ and the Ampere's law becomes $\nabla^2\mathbf{A} = -\delta\mathbf{J}$. Again, by ignoring the small gradient on the equilibrium quantities we have $\delta\mathbf{J}\cdot\mathbf{B} \simeq -\nabla^2(\mathbf{A}\cdot\mathbf{B}) = \nabla^2(\mathbf{B}\cdot\boldsymbol{\nabla}\Phi)$. Moreover, we consider the wave frequency to be much smaller than the compressional wave frequency ($\sim k_\perp V_A$, where $V_A = B/\rho^{1/2}$ is the Alfvén speed), so that to the lowest order in $(\omega/k_\perp V_A)$, $\boldsymbol{\nabla}_\perp(\delta P + \delta\mathbf{B}\cdot\mathbf{B}) \simeq 0$ [*Cheng and Johnson*, 1999]. Then, from Eq. (1) and $\boldsymbol{\nabla}\cdot\delta\mathbf{J} = \mathbf{B}\cdot\boldsymbol{\nabla}(\delta\mathbf{J}\cdot\mathbf{B}/B^2) + \boldsymbol{\nabla}\cdot\delta\mathbf{J}_\perp = 0$, we obtain the vorticity equation

$$\mathbf{B}\cdot\boldsymbol{\nabla}\left(\frac{\nabla_\perp^2(\mathbf{B}\cdot\boldsymbol{\nabla}\Phi)}{B^2}\right) + \frac{\rho\omega^2}{B^2}\nabla_\perp^2\Phi - \frac{2\boldsymbol{\kappa}\times\mathbf{B}\cdot\boldsymbol{\nabla}\delta P}{B^2} \simeq 0. \tag{2}$$

From the adiabatic pressure law, we obtain $\delta P - \mathbf{B}\times\boldsymbol{\nabla}P\cdot\boldsymbol{\nabla}\Phi/B^2 + \Gamma_s P\boldsymbol{\nabla}\cdot\boldsymbol{\xi} \simeq 0$, where we have made use of $\boldsymbol{\xi}\cdot\boldsymbol{\nabla}P = (i\delta\mathbf{E}\times\mathbf{B}/\omega B^2)\cdot\boldsymbol{\nabla}P \simeq -\mathbf{B}\times\boldsymbol{\nabla}P\cdot\boldsymbol{\nabla}\Phi/B^2$.

Next, we evaluate $\boldsymbol{\nabla}\cdot\boldsymbol{\xi} = \mathbf{B}\cdot(\boldsymbol{\xi}\cdot\mathbf{B}/B^2) + \boldsymbol{\nabla}\cdot\boldsymbol{\xi}_\perp$. By operating the momentum equation with $\mathbf{B}\cdot$ we obtain an expression for the parallel displacement $\rho\omega^2\boldsymbol{\xi}\cdot\mathbf{B} \simeq \mathbf{B}\cdot\boldsymbol{\nabla}\delta P - \mathbf{B}\times\boldsymbol{\nabla}P\cdot\boldsymbol{\nabla}\left(\mathbf{B}\cdot\boldsymbol{\nabla}\Phi\right)/B^2$, where we evaluate $\delta\mathbf{B}\cdot\boldsymbol{\nabla}P = \boldsymbol{\nabla}\cdot(\mathbf{A}\times\boldsymbol{\nabla}P) \simeq \boldsymbol{\nabla}\cdot[(\mathbf{A}\cdot\mathbf{B}/B^2)\mathbf{B}\times\boldsymbol{\nabla}P] \simeq -(\mathbf{B}\times\boldsymbol{\nabla}P/B^2)\cdot\boldsymbol{\nabla}(\mathbf{B}\cdot\boldsymbol{\nabla}\Phi)$ with the help of $\mathbf{A}\cdot\mathbf{B} = -\mathbf{B}\cdot\boldsymbol{\nabla}\Phi$ due to the vanishing parallel electric field. Making use of the Ohm's law, we obatin

$$\boldsymbol{\nabla}\cdot\boldsymbol{\xi}_\perp = -\left(\frac{2\boldsymbol{\kappa}\times\mathbf{B}}{B^2} + \frac{\mathbf{B}\times\boldsymbol{\nabla}P}{B^4}\right)\cdot\boldsymbol{\nabla}_\perp\Phi - \frac{\delta\mathbf{B}\cdot\mathbf{B}}{B^2}. \tag{3}$$

Finally from Eqs. (2)-(3) and $\delta P + \delta\mathbf{B}\cdot\mathbf{B} = 0$, and eliminating $\delta P$, we obtain two 3D eigenmode equations for $\Phi$ and $\boldsymbol{\nabla}\cdot\boldsymbol{\xi}$ for describing low frequency modes with perpendicular wavelength much shorter than the parallel wavelength:

$$\begin{aligned}\mathbf{B}\cdot\boldsymbol{\nabla}\left(\frac{\nabla_\perp^2(\mathbf{B}\cdot\boldsymbol{\nabla}\Phi)}{B^2}\right) + \frac{\rho\omega^2}{B^2}\nabla_\perp^2\Phi \\ -\frac{2\boldsymbol{\kappa}\times\mathbf{B}}{B^2}\cdot\boldsymbol{\nabla}\left(\frac{\mathbf{B}\times\boldsymbol{\nabla}P\cdot\boldsymbol{\nabla}\Phi}{B^2}\right) = \frac{2\boldsymbol{\kappa}\times\mathbf{B}\cdot\boldsymbol{\nabla}(\Gamma_s P\boldsymbol{\nabla}\cdot\boldsymbol{\xi})}{B^2},\end{aligned} \tag{4}$$

and

$$\begin{aligned}\mathbf{B}\cdot\boldsymbol{\nabla}\left[\frac{\Gamma_s P}{\rho\omega^2 B^2}\mathbf{B}\cdot\boldsymbol{\nabla}(\boldsymbol{\nabla}\cdot\boldsymbol{\xi})\right] + \frac{\Gamma_s P + B^2}{B^2}\boldsymbol{\nabla}\cdot\boldsymbol{\xi} \\ = \frac{2\boldsymbol{\kappa}\times\mathbf{B}\cdot\boldsymbol{\nabla}\Phi}{B^2}.\end{aligned} \tag{5}$$

It is clear that these two equations describe the coupling between the shear Alfvén type modes, which are mainly determined by Eq. (4), and the slow magnetosonic type modes, which are mainly determined by Eq. (5). The coupling is mainly via the magnetic field curvature and the plasma pressure.

### 2.1. MHD Ballooning Mode Equations

Equations (4) and (5) describe low frequency modes in the three-dimensional space and are usually difficult to solve if not impossible. Thus, further approximations must be made to simplify these two equations. Fortunately a so-called WKB-ballooning formalism has been developed to simplify these equations by taking advantage of the nature of

solutions that the perpendicular wavelength is much shorther than the parallel wavelength [*Dewar and Glasser*, 1983; *Nevins and Pearlstein*, 1988; *Dewar et al.*, 2001]. Adopting the WKB-ballooning formalism, we consider the eikonal representation of the perturbed quantities, $\Phi = ie^{iS}\hat{\Phi}$, where $S \gg 1$ is the WKB eikonal and $\mathbf{B}\cdot\boldsymbol{\nabla}S = 0$. Note that $\boldsymbol{\nabla}S$ is essentially the wave vector perpendicular to $\mathbf{B}$. Thus, the fast variation of $\Phi$ in the direction perpendicular to $\mathbf{B}$ is contained in $e^{iS}$ and $\hat{\Phi}$ describes the slow variation along as well as perpendicular to $\mathbf{B}$. Then, to the lowest order in $1/S \ll 1$, the MHD vorticity equation, Eq. (4), reduces to

$$\mathbf{B}\cdot\boldsymbol{\nabla}\left(\frac{|\boldsymbol{\nabla}S|^2\mathbf{B}\cdot\boldsymbol{\nabla}\hat{\Phi}}{B^2}\right) + \frac{\rho\omega^2}{B^2}\nabla_\perp^2\hat{\Phi} + \kappa_c P_s\hat{\Phi} + \kappa_c(\Gamma_s P\Delta) = 0, \tag{6}$$

where $\kappa_c = 2\boldsymbol{\kappa}\times\mathbf{B}\cdot\boldsymbol{\nabla}S/B^2$, $P_s = \boldsymbol{\nabla}P\times\mathbf{B}\cdot\boldsymbol{\nabla}S/B^2$, and $\boldsymbol{\nabla}\cdot\boldsymbol{\xi} = e^{iS}\Delta$. Similarly, Eq. (5) reduces to

$$\mathbf{B}\cdot\boldsymbol{\nabla}\left[\frac{\Gamma_s P}{\rho\omega^2 B^2}\mathbf{B}\cdot\boldsymbol{\nabla}\Delta\right] + \frac{\Gamma_s P + B^2}{B^2}\Delta + \kappa_c\hat{\Phi} = 0. \tag{7}$$

Eqs. (6) and (7) are 1D equations along $\mathbf{B}$, and the eigenvalues depend on the angle between $\boldsymbol{\nabla}S$ and $\boldsymbol{\nabla}P$. With the Euler potential representation of the ambient magnetic field $\mathbf{B} = \boldsymbol{\nabla}\psi\times\boldsymbol{\nabla}\alpha$, $\boldsymbol{\nabla}S$ can be expressed as $\boldsymbol{\nabla}S = S_\psi\boldsymbol{\nabla}\psi + S_\alpha\boldsymbol{\nabla}\alpha$, where $S_\psi = \partial S/\partial\psi$, and $S_\alpha = \partial S/\partial\alpha$. Then, $\kappa_c = 2S_\alpha[\kappa_s(\boldsymbol{\nabla}\psi\cdot\boldsymbol{\nabla}\alpha/|\boldsymbol{\nabla}\psi|^2 + \Upsilon/\psi) - \kappa_\psi]$, and $P_s = S_\alpha[(\Upsilon/\psi)\partial P/\partial\alpha - \partial P/\partial\psi]$, where $\kappa_\psi = \boldsymbol{\kappa}\cdot\boldsymbol{\nabla}\psi/|\boldsymbol{\nabla}\psi|^2$, $\kappa_s = \boldsymbol{\kappa}\cdot\mathbf{B}\times\boldsymbol{\nabla}\psi/B^2$, and $\Upsilon = \psi S_\psi/S_\alpha$ is a dimensionless free parameter. We see that $S_\alpha$ can be combined with $\hat{\Phi}$, and the eigenmode equations, Eqs. (6) and (7) depend on $\Upsilon$. Thus, the lowest order eigenvalue, $\omega^2$, is a function of $\Upsilon$ and field lines labeled by $\psi$ and $\alpha$, with a corresponding wave structure along the field line. $\Upsilon$ has two physical meanings; first, it can be considered as the ratio of the radial wave vector to the azimuthal wave vector, and second, it represents the central location of the mode structure along the field line. Thus, by scanning the dependence of $\omega^2$ on $\Upsilon$ we determine the radial wave vector and its

localization location along the field line for the most unstable mode. We will address the lowest order ballooning mode equations and find out the lowest order eigenvalue for each field line. From numerical solutions for magnetospheric equilibria with a north-south symmetry, the most unstable solution is obtained with $\Upsilon = 0$ for each field line.

To solve the lowest order ballooning mode equations, Eqs. (6) and (7), we onstruct a variational principle. Multiplying Eq.(6) by $\hat{\Phi}^*$ (the complex conjugate of $\hat{\Phi}$) and subtracting it by the complex conjugate of Eq.(7) multiplied by $\Gamma_s P\Delta$, and then integrating along the field line with respect to $ds/B$, where s denotes the distance along the field line, we obtain a Lagrangian functional $\delta L$ given by

$$\delta L = \int_{s_1}^{s_2} \frac{ds}{B} \left\{ \rho\omega^2 \left( \frac{|\boldsymbol{\nabla} S|^2}{B^2} |\hat{\Phi}|^2 + B^2 |Z|^2 \right) + \kappa_c P_s |\hat{\Phi}|^2 \right.$$
$$\left. - \left[ \frac{|\boldsymbol{\nabla}\psi|^2}{B^2} |\mathbf{B}\cdot\boldsymbol{\nabla}\hat{\Phi}|^2 + \frac{\Gamma_s P B^2}{\Gamma_s P + B^2} |\kappa_c \hat{\Phi} + \mathbf{B}\cdot\boldsymbol{\nabla} Z|^2 \right] \right\} = 0 \qquad (8)$$

where $s_1$ and $s_2$ are the two end points of the field line anchored in the ionosphere, $Z = \Gamma_s P(\mathbf{B}\cdot\boldsymbol{\nabla}\Delta)/\rho\omega^2 B^2$, the boundary conditions at the field line end points are assumed to be $\hat{\Phi}^* \mathbf{B}\cdot\boldsymbol{\nabla}\hat{\Phi} = 0$ and $\Delta Z^* = 0$, and we have also made use of Eq. (7) to substitute $\Delta$ in terms of $\hat{\Phi}$ and $\mathbf{B}\cdot\boldsymbol{\nabla} Z$. It is straightforward to verify that Eqs. (6) and (7) are a consequence of the requirement that the functional $\delta L$ is stationary. Since $\delta L = 0$, it is clear that the eigenvalues $\omega^2$ and the corresponding eigenfunctions $\hat{\Phi}$ and $\Delta$ must be real. The determination of the stability of ballooning modes reduces to that of finding the eigenvalues $\omega^2$ and eigenfunctions so that the Lagrangian functional $\delta L$ is stationary with respect to variations of $\hat{\Phi}$ and $\Delta$. The admissible variational functions must be square-integrable and satisfy the boundary conditions at the field line end points. It should be noted from Eq. (8) that there is a possibility of $\omega^2 < 0$ if $\kappa_c P_s > 0$, and if $\omega^2 < 0$ the plasma is unstable at these field lines. From the definition of $\kappa_c$ and $P_s$ (given after Eq. (6)) we see that if the pressure gradient is in the same direction as the magnetic field curvature, then $\kappa_c P_s > 0$ and the ballooning mode is possible to be unstable.

**Figure 1.**

**Figure 2.**

### 2.2. Numerical Solutions of MHD Ballooning Mode Equations

Once a 3D quasi-static magnetospheric equilibrium is known we can compute the ballooning mode solutions for each field line. However, to obtain the mode frequency or growth rate in physical unit we need to specify the mass density along field lines. We assume for simplicity the plasma density to be constant along the field line and choose it to be a function of radius in the equatorial plane: $\rho(R) = 10\,(R_{geos}/R)^3 m_p/cm^3$, where $R_{geos} = 6.6\,R_E$ is the geosynchronous orbit distance and $m_p$ is the proton mass. When the actual mass density distribution is known, the frequency or growth rate can be recalculated easily with the actual density from the results given in this paper.

Employing the growth phase magnetospheric equilibrium published previously [*Zaharia and Cheng*, 2003] and choosing $(S_\psi/S_\alpha) = 0$, we compute numerically the eigenvalues $\omega^2$ and the eigenfunctions by solving the Lagrangian equation, Eq. (8) for each field line by a finite element method with the boundary conditions that both $\hat{\Phi}$ and $\Delta$ vanish at the end points of the field line in the ionosphere. Figures 1 and 2 show the color plot in the equatorial plane and the contours in the northern polar ionosphere of the eigenvalue $f^2$ (in $(mHz)^2$) of the fundamental harmonic ballooning modes, respectively. Also shown in Fig. 1 is the contours of the azimuthal current density (in $nA/m^2$) and in Fig. 2 is the color plot of the field-aligned current density. Note that all field lines beyond $x \simeq -6\,\mathrm{R_E}$ down the tail in the night side are unstable. The region of the most unstable modes tracks well with the strong cross-tail current sheet region, consistent with the expectation from substorm onset observations. The peak growth rate region is located in the tailward side of the strong cross-tail current region. In the polar ionosphere the field lines in the peak ballooning instability growth rate region map to the transition region between the region-1 and region-2 currents. The results clearly indicate that, although the ideal MHD model over estimates the instability growth rate due to the lack of particle kinetic effects, it shows the field lines where the ballooning free energy is largest and the most unstable ballooning mode is located. Moreover, we expect that the global structure

of the MHD ballooning instability is localized around the maximum growth rate location in the equatorial plane with an half-width extending to the location with growth rate equal to about one half of the maximum growth rate. **Figure 3.**

Next, we compute the stability of the ballooning modes for the same growth phase magnetospheric equilibrium with the Lee-Wolf model [*Lee and Wolf*, 1992] and the fast-MHD model [*Horton et al.*, 1999], which made approximations on the plasma compressibility, and compare these solutions with the solution of the full MHD model shown in Figs. 1 and 2. This will resolve the controversy arising from these approximations [*Lee*, 1999]. In the Lee-Wolf model, the plasma compressibility is assumed to be a non-vanishing constant along the field line. With $\mathbf{B}\cdot\boldsymbol{\nabla}\Delta = 0$, $\Delta$ can be obtained from Eq. (7) and is given by $\langle(\Gamma_s P + B^2)/B^2\rangle\Delta + \langle\kappa_c\hat{\Phi}\rangle = 0$, where $\langle X\rangle = \int_{s_1}^{s_2} dsX/B$. Then, Eq. (6) reduces to

$$\mathbf{B}\cdot\boldsymbol{\nabla}\left(\frac{|\boldsymbol{\nabla}S|^2\mathbf{B}\cdot\boldsymbol{\nabla}\hat{\Phi}}{B^2}\right) + \frac{\rho\omega^2}{B^2}\nabla_\perp^2\hat{\Phi} + \kappa_c P_s\hat{\Phi} - \frac{\kappa_c\Gamma_s P\langle\kappa_c\hat{\Phi}\rangle}{\langle\frac{\Gamma_s P+B^2}{B^2}\rangle} = 0, \tag{9}$$

and a Lagrangian functional $\delta L$ can be constructed and is given by

$$\delta L = \int_{s_1}^{s_2}\frac{ds}{B}\left\{\rho\omega^2\left(\frac{|\boldsymbol{\nabla}S|^2}{B^2}|\hat{\Phi}|^2\right) + \kappa_c P_s|\hat{\Phi}|^2 - \left[\frac{|\boldsymbol{\nabla}S|^2}{B^2}|\mathbf{B}\cdot\boldsymbol{\nabla}\hat{\Phi}|^2 + \frac{\Gamma_s P\kappa_c\hat{\Phi}\langle\kappa_c\hat{\Phi}\rangle}{\langle\frac{\Gamma_s P+B^2}{B^2}\rangle}\right]\right\} = 0 \tag{10}$$

The solution of Eq. (10) is shown in Fig. 3, which shows that ballooning modes are unstable only near the current sheet region between $X = -8$ and $-10\,\mathrm{R_E}$, but are stable in other region. This result is different from the full MHD solution shown in Figure 1. Thus, the Lee-Wolf model produce too much stabilization due to the approximation of constant plasma compressibility. **Figure 4.**

In the fast-MHD model [*Horton et al.*, 1999], the parallel displacement is assumed to vanish, $\boldsymbol{\xi}\cdot\mathbf{B} = 0$. From the adiabatic pressure law and the parallel component of the

momentum equation, we obtain $\Delta + [\kappa_c B^2/(\Gamma_s P + B^2)]\hat{\Phi} = 0$. Then, Eq. (6) reduces to

$$\mathbf{B}\cdot\boldsymbol{\nabla}\left(\frac{|\boldsymbol{\nabla}S|^2\mathbf{B}\cdot\boldsymbol{\nabla}\hat{\Phi}}{B^2}\right) + \frac{\rho\omega^2}{B^2}\nabla_\perp^2\hat{\Phi} + \kappa_c P_s\hat{\Phi} - \frac{\Gamma_s P\kappa_c^2 B^2}{\Gamma_s P + B^2}\hat{\Phi} = 0, \tag{11}$$

and a Lagrangian functional $\delta L$ can be constructed and is given by

$$\delta L = \int_{s_1}^{s_2}\frac{ds}{B}\left\{\rho\omega^2\left(\frac{|\boldsymbol{\nabla}S|^2}{B^2}|\hat{\Phi}|^2\right) + \kappa_c P_s|\hat{\Phi}|^2 - \left[\frac{|\boldsymbol{\nabla}S|^2}{B^2}|\mathbf{B}\cdot\boldsymbol{\nabla}\hat{\Phi}|^2 + \frac{\Gamma_s P\kappa_c^2 B^2}{\Gamma_s P + B^2}|\hat{\Phi}|^2\right]\right\} = 0 \tag{12}$$

The solution of Eq. (12) is shown in Fig. 4. which clearly shows that for most of the field lines (except near the far tail boundary of the equilibrium) the ballooning modes are stable. This result is completely different from the results of full MHD model shown in Figures 1 and those of the Lee-Wolf model shown in Fig. 3. Thus, the fast-MHD model gives a much worse approximation of the plasma compressibility.

## 3. Summary and Discussion

In summary, based on the ideal MHD model the ballooning modes are expected to be unstable for the growth phase magnetospheric equilibrium in a large region of the plasma sheet where $\beta_{eq} \geq 1$. The most unstable region is located in the strong cross-tail current sheet region, which maps into the ionosphere in the transition area between the region-1 and region-2 currents. The numerical results clearly illustrate that to obtain the correct stability result even within the ideal MHD model it is essential to model the plasma compressibility correctly as well as the equilibrium fields realistically. Moreover, even for quiet time equilibria [*Zaharia et al.*, 2003], the full MHD calculations (not shown in the paper) indicate that the ballooning modes are unstable for the entire plasma sheet region when $\beta_{eq} \geq 1$.

The results of the ideal MHD ballooning mode stability calculations are not consistent with the AMPTE/CCE observations that during most of the growth phase

$\beta_{eq} < 50$ and the magnetic fields are quiet without noticeable fluctuations [*Lui et al.*, 1992], and the low frequency instability was observed in the enhanced cross-tail current sheet region only toward the end of the growth phase when $\beta_{eq} > 50$ [*Cheng and Lui*, 1998]. Moreover, the ideal MHD model would predict purely growing ballooning instabilities, and thus can not explain the observed frequency of the instability. Another fundamental difficulty of the ideal MHD model is that there is no parallel electric field, and thus the unstable MHD ballooning mode does not accelerate particles to produce the substorm onset auroral brightening as observed in the ionosphere. However, even with these inconsistencies with observations, the ideal MHD model provides the valuable information that the most unstable ballooning instability and the maximum free energy associated with the product of the plasma pressure gradient and magnetic field curvature are located in the strong cross-tail current sheet region when realistic 3D magnetospheric equilibria are considered.

To mitigate these difficulties arising from the ideal MHD model, we need to consider the particle kinetic effects. As was shown previously [*Cheng and Lui*, 1998], the kinetic effects of ion gyroradii and trapped electron dynamics can greatly increase the stabilizing effects of field line tension and thus enhance the critical $\beta$ to excite the ballooning instability. The consequence is to reduce the equatorial region of the unstable ballooning modes to the strong cross-tail current sheet region, where the free energy for the ballooning instability is maximum. Full kinetic calculations need to be carried out to provide a quantitative conclusion.

**Acknowledgments.** This work is supported by the NASA grant No. W-10062 and the DoE Contract No. DE-AC02-76-CHO3073.

## References

Cheng, C. Z., and J. R. Johnson, A kinetic-fluid model, *J. Geophys. Res.*, *104*, 413–427, 1999.

Cheng, C. Z., and A. T. Y. Lui, Kinetic ballooning instability for substorm onset and current disruption observed by AMPTE/CCE, *Geophys. Res. Lett.*, *25*, 4091–4094, 1998.

Dewar, R. L., and A. H. Glasser, Ballooning mode spectrum in general toroidal systems, *Phys. Fluids*, *26*, 3038, 1983.

Dewar, R. L., P. Cuthbert, and R. Ball, Strong quantum chaos in the global ballooning mode spectrum of three-dimensional plasmas, *Phys. Rev. Lett.*, *86*, 2321, 2001.

Erickson, G. M., N. C. Maynard, W. J. Burke, G. R. Wilson, and M. A. Heinemann, Electromagnetics of substorm onsets in the near-geosynchronous plasma sheet, *J. Geophys. Res.*, *105*, 25265–25290, 2000.

Horton, W., H. V. Wong, and J. W. Van Dam, Substorm trigger conditions, *J. Geophys. Res.*, *104*, 22745, 1999.

Hurricane, O. A., MHD ballooning stability of a sheared plasma sheet, *J. Geophys. Res.*, *102*, 19903, 1997.

Kan, J., On the structure of the magnetotail current sheet, *J. Geophys. Res.*, *78*, 3773, 1973.

Lee, D. Y., Ballooning instability in the tail plasma sheet, *Geophys. Res. Lett.*, *25*, 4095, 1998.

Lee, D. Y., Effect of plasma compression on plasma sheet stability, *Geophys. Res. Lett.*, *26*, 2705, 1999.

Lee, D. Y., and R. A. Wolf, Is the Earth's magnetotail balloon unstable?, *J. Geophys. Res.*, *97*, 19251, 1992.

Lui, A. T. Y., et al., Current disruptions in the near-Earth neutral sheet region, *J. Geophys. Res.*, *97*, 1461, 1992.

Nevins, W. M., and L. D. Pearlstein, Moderate-m ballooning modes in quadrapole stabilized tandem mirrors, *Phys. Fluids*, *31*, 1988, 1988.

Ohtani, S., K. Takahashi, L. J. Zanetti, T. A. Potemra, R. W. McEntire, and T. Iijima, Tail current disruption in the geosynchronous region, edited by J. R. Kan, T. A. Potemra, S. Kokubun, and T. Iijima, in *AGU monograph on Magnetospheric Substorms*, pp. 131–137. AGU, Washington, D. C., 1991.

Roux, A., S. Perraut, A. Morane, P. Robert, A. Korth, G. .Kremser, A. Pederson, R. Pellinen, and Z. Y. Pu, Plasma sheet instability related to the westward traveling surge, *J. Geophys. Res.*, *96*, 17697, 1991.

Voigt, G.-H., Field line twist and field-aligned currents in an axisymmetric equilibrium magnetosphere, *J. Geophys. Res.*, *91*, 10995, 1986.

Zaharia, S., and C. Z. Cheng, Near-Earth thin current sheets and Birkeland currents during substorm growth phase, *Geophys. Res. Lett.*, *30(17)*, 1883, doi:10.1029/2003GL017456, 2003.

Zaharia, S., C. Z. Cheng, and K. Maezawa, 3D force balanced magnetospheric configurations, *Ann. Geophys.*, *21*, paper number – AG03014, in press, 2003.

---

This manuscript was prepared with the AGU LaTeX macros v3.0.

With the extension package 'AGU$^{++}$', version 1.2 from 1995/01/12

## Figure Captions

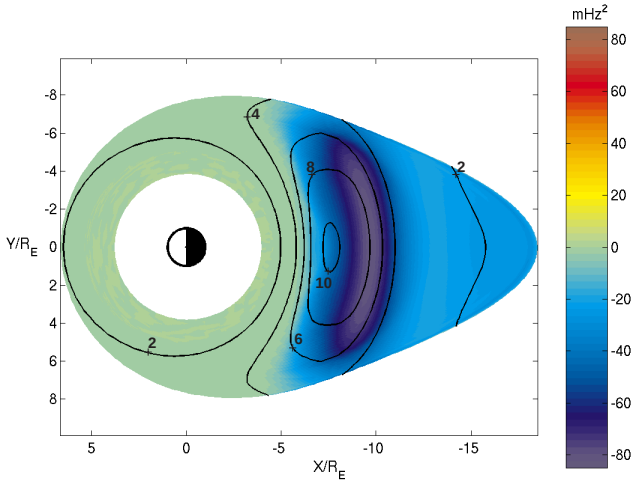


**Figure 1.** The square of frequency (in $(mHz)^2$) of ballooning modes is shown in color in the equatorial plane for the growth phase equilibrium with the full MHD model. The contours of the azimuthal current density (in $nA/m^2$) is also plotted to show the location of the most unstable region relative to the strong cross-tail current region.

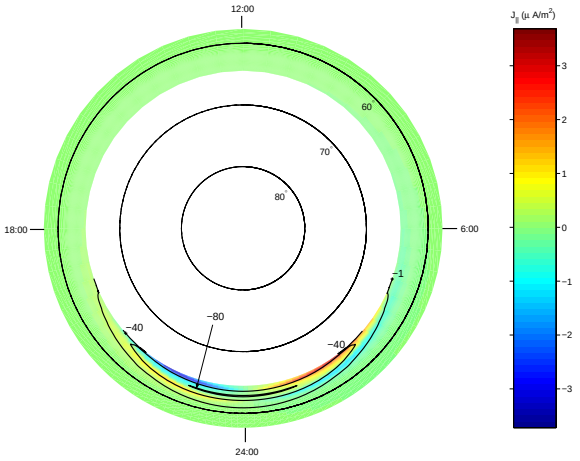


**Figure 2.** The contours of the square of frequency (in $(mHz)^2$) of ballooning modes is plotted over the northern polar ionosphere for the growth phase equilibrium with the full MHD model. The field-aligned current density is also shown in color to show that the most unstable ballooning instability region is located at the transition region between the region-1 and region-2 currents.

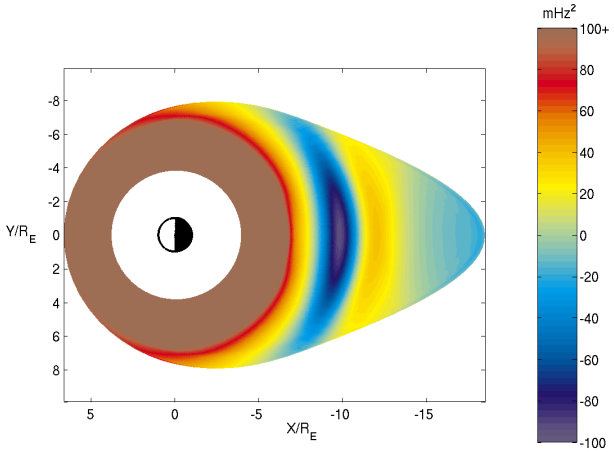


**Figure 3.** The square of frequency (in $(mHz)^2$) of ballooning modes is plotted in the equatorial plane for the growth phase equilibrium with the Lee-Wolf model of compressibility.

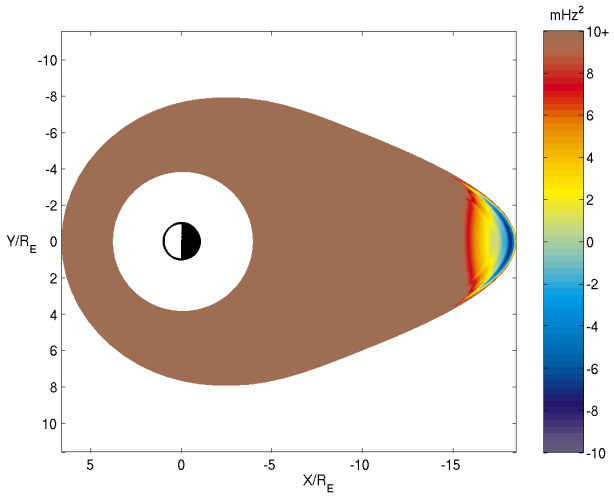


**Figure 4.** The square of frequency (in $(mHz)^2$) of ballooning modes is plotted over the equatorial plane for the growth phase equilibrium with the fast-MHD model of compressibility.

## External Distribution

Plasma Research Laboratory, Australian National University, Australia

Professor I.R. Jones, Flinders University, Australia

Professor João Canalle, Instituto de Fisica DEQ/IF - UERJ, Brazil

Mr. Gerson O. Ludwig, Instituto Nacional de Pesquisas, Brazil

Dr. P.H. Sakanaka, Instituto Fisica, Brazil

The Librarian, Culham Laboratory, England

Mrs. S.A. Hutchinson, JET Library, England

Professor M.N. Bussac, Ecole Polytechnique, France

Librarian, Max-Planck-Institut für Plasmaphysik, Germany

Jolan Moldvai, Reports Library, Hungarian Academy of Sciences, Central Research Institute for Physics, Hungary

Dr. P. Kaw, Institute for Plasma Research, India

Ms. P.J. Pathak, Librarian, Institute for Plasma Research, India

Ms. Clelia De Palo, Associazione EURATOM-ENEA, Italy

Dr. G. Grosso, Instituto di Fisica del Plasma, Italy

Librarian, Naka Fusion Research Establishment, JAERI, Japan

Library, Laboratory for Complex Energy Processes, Institute for Advanced Study, Kyoto University, Japan

Research Information Center, National Institute for Fusion Science, Japan

Dr. O. Mitarai, Kyushu Tokai University, Japan

Dr. Jiangang Li, Institute of Plasma Physics, Chinese Academy of Sciences, People's Republic of China

Professor Yuping Huo, School of Physical Science and Technology, People's Republic of China

Library, Academia Sinica, Institute of Plasma Physics, People's Republic of China

Librarian, Institute of Physics, Chinese Academy of Sciences, People's Republic of China

Dr. S. Mirnov, TRINITI, Troitsk, Russian Federation, Russia

Dr. V.S. Strelkov, Kurchatov Institute, Russian Federation, Russia

Professor Peter Lukac, Katedra Fyziky Plazmy MFF UK, Mlynska dolina F-2, Komenskeho Univerzita, SK-842 15 Bratislava, Slovakia

Dr. G.S. Lee, Korea Basic Science Institute, South Korea

Institute for Plasma Research, University of Maryland, USA

Librarian, Fusion Energy Division, Oak Ridge National Laboratory, USA

Librarian, Institute of Fusion Studies, University of Texas, USA

Librarian, Magnetic Fusion Program, Lawrence Livermore National Laboratory, USA

Library, General Atomics, USA

Plasma Physics Group, Fusion Energy Research Program, University of California at San Diego, USA

Plasma Physics Library, Columbia University, USA

Alkesh Punjabi, Center for Fusion Research and Training, Hampton University, USA

Dr. W.M. Stacey, Fusion Research Center, Georgia Institute of Technology, USA

Dr. John Willis, U.S. Department of Energy, Office of Fusion Energy Sciences, USA

Mr. Paul H. Wright, Indianapolis, Indiana, USA

The Princeton Plasma Physics Laboratory is operated
by Princeton University under contract
with the U.S. Department of Energy.

Information Services
Princeton Plasma Physics Laboratory
P.O. Box 451
Princeton, NJ 08543

Phone: 609-243-2750
Fax: 609-243-2751
e-mail: pppl_info@pppl.gov
Internet Address: http://www.pppl.gov